Polymer Composites

WILEY | spe INSPIRING PLASTICS PROFESSIONALS

RESEARCH ARTICLE

Effect of Fiber Orientation on the Properties of Continuous Glass Fiber Reinforced PLA Composites Produced via Nozzle-Impregnation 3D Printing

Ahmet Cagri Kilinc[1] | Turker Turkoglu[2] | Volkan Arikan[1] | Sare Celik[2] | Fidan Bilir Kilinc[3] | Selcuk Yesiltepe[1]

[1]Department of Mechanical Engineering, Osmaniye Korkut Ata University, Osmaniye, Turkey | [2]Department of Mechanical Engineering, Balıkesir University, Balıkesir, Turkey | [3]Department of Textile Engineering, Graduate School of Natural and Applied Sciences, Ege University, Izmir, Turkey

Correspondence: Ahmet Cagri Kilinc (ahmetcagrikilinc@osmaniye.edu.tr)

Received: 2 June 2025 | **Revised:** 4 August 2025 | **Accepted:** 15 August 2025

Keywords: 3D printing | continuous fiber | fiber orientation | mechanical properties | nozzle-impregnation

ABSTRACT

In this study, continuous glass fiber-reinforced PLA composites were fabricated via a custom-designed dual-feed FDM system using a nozzle-impregnation method. PLA filament and glass fiber tow were co-fed into the extruder, where fiber impregnation occurred before deposition through a rounded steel nozzle. Specimens with fiber orientations of 0°, 0/90°, 90°, ±45°, and ±20° were printed using a 0.5 mm layer height and 2 mm line width. Thermogravimetric analysis revealed that fiber addition slightly decreased the onset degradation temperature of the matrix. Ignition loss measurements confirmed that fiber orientation had no effect on fiber volume fraction (~12.5 vol.%). Tensile and flexural strengths increased significantly as fiber alignment approached 0°, reaching 82.75 MPa and 48.04 MPa, respectively, while 90°-oriented samples showed the lowest values. Scanning Electron Microscope analysis revealed poor impregnation and interfacial bonding in off-axis configurations. Finite element simulations showed a strong correlation with experimental modulus values for both 0° and 90° orientations. Furthermore, increasing fiber volume fraction was found to enhance stiffness along the fiber axis, confirming the anisotropic nature of the material and emphasizing the importance of fiber alignment. This study provides a scalable approach for tailoring mechanical performance in additively manufactured continuous fiber composites.

1 | Introduction

Additive manufacturing (AM), particularly Fused Deposition Modeling (FDM), has transformed the landscape of polymer processing by enabling the production of complex geometries with high customization and material efficiency [1–3]. Among commonly used thermoplastics, polylactic acid (PLA) stands out for its biodegradability, affordability, and ease of processing [4, 5]. However, its limited mechanical strength and brittle behavior restrict its use in functional or load-bearing applications [6, 7].

To address these shortcomings, continuous fiber reinforcements have garnered attention due to their superior ability to improve stiffness, strength, and impact resistance [8, 9]. Glass fiber (GF), in particular, offers a desirable combination of tensile strength, thermal stability, and cost-effectiveness. Traditionally, GF-reinforced composites have been produced using techniques such as hand lay-up or vacuum infusion. While these methods provide good fiber impregnation and are widely adopted in industrial settings, they present notable limitations, including labor-intensive processing, limited geometric complexity, poor scalability, and challenges in achieving repeatable quality in thin or complex structures [10–12].

While many studies have investigated the macro- and microscale mechanical behavior of fiber-reinforced composites—particularly in the automotive sector—most focus on conventional laminated textile structures or randomly oriented

Summary

- Continuous GF/PLA composites were produced via dual-feed FDM printing.
- Fiber orientation had a strong effect on tensile and flexural strength.
- 0° orientation showed the highest mechanical performance among all angles.
- FEA accurately predicted elastic response for 0° and 90° orientations.
- Stiffness increased with fiber volume along the fiber alignment direction.

short fibers integrated through thermoset-based systems [13–15]. These approaches often prioritize enhanced stiffness, thermal resistance, and vibration damping but do not fully leverage the design freedom and functional grading potential offered by additive manufacturing [16]. Moreover, recent works have emphasized the importance of interfacial morphology, fiber–matrix adhesion, and structural architecture in dictating impact energy absorption and viscoelastic response, yet such considerations remain underexplored in the context of continuous glass fiber-reinforced thermoplastics fabricated via direct-feed FDM systems [17].

In contrast, FDM-based approaches offer a promising route for fabricating GF-reinforced composites with enhanced geometrical freedom, reduced material waste, and integration with digital design workflows [18, 19]. By feeding the PLA matrix filament and continuous glass fiber simultaneously into the printer's heated nozzle, it becomes possible to fabricate composite parts in a layer-wise fashion without the need for pre-impregnated filaments or post-curing steps. This method enables direct control over fiber placement and alignment, which is critical to mechanical performance [4, 20–22].

Gavande et al. [8] investigated the mechanical performance of continuous glass fiber-reinforced thermoplastic composites manufactured via vacuum infusion. The resulting laminates exhibited superior mechanical properties compared to their epoxy-based counterparts, including notable improvements in compressive, tensile, and shear strengths. Most significantly, the residual compressive strength after low-velocity impact was 142% higher than that of the epoxy composites. While the study confirms the feasibility of producing high-performance thermoplastic composites through conventional vacuum infusion, it also highlights the geometric limitations associated with mold-dependent fabrication methods. Complementing this, Billah et al. [23] investigated the thermomechanical behavior of short carbon fiber (CF) and short glass fiber (GF) reinforced ABS composites specifically designed for large-format additive manufacturing (LFAM). Their comprehensive characterization demonstrated that fiber reinforcement enhances stiffness, thermal stability, and dimensional control compared to neat ABS. Notably, ABS/CF exhibited a 272% increase in stiffness. However, unlike the present study, which utilizes continuous glass fiber reinforcement, their work focused solely on short fiber composites, which exhibit different reinforcement mechanisms and stress transfer behaviors. This distinction is critical when assessing the structural capabilities of fiber-reinforced thermoplastics produced via extrusion-based methods. In a related context, Dou et al. [24] systematically examined the influence of key process parameters—layer height, extrusion width, printing temperature, and printing speed—on the tensile mechanical properties of continuous carbon fiber-reinforced PLA composites produced via a modified FDM 3D printer. Their results indicated that relative fiber content, governed by layer height and extrusion width, plays the most significant role in determining tensile strength and stiffness, with values reaching up to 243.5 MPa and 25.8 GPa, respectively. Although temperature and speed affected the fiber-matrix interface, their impact was secondary. Notably, the primary failure mode was fiber pull-out due to weak interfacial bonding. Despite methodological similarities, their use of continuous carbon fiber introduces different interfacial behavior and stiffness characteristics compared to the continuous glass fiber reinforcement examined in the current work.

Recent studies have explored continuous fiber reinforcement in polymers, particularly with carbon and aramid fibers [24, 25]. Despite the increasing interest in continuous fiber-reinforced composites manufactured via additive processes, most studies to date have primarily focused on carbon fiber reinforcement due to its high stiffness and strength. In contrast, continuous glass fiber—despite being more cost-effective and offering excellent mechanical and thermal stability—remains relatively underexplored, particularly in combination with PLA matrices and direct-feed FDM technologies. The literature includes a limited number of studies utilizing in-nozzle impregnation techniques with dual-feed extrusion systems, where achieving uniform fiber wet-out, controlling fiber alignment, and ensuring strong interfacial bonding remain critical challenges. Furthermore, many existing approaches rely on prepreg-based feedstocks or involve substantial modifications to the printhead architecture, which complicate the process, increase production costs, and hinder scalability for industrial applications. These limitations highlight a clear research gap in the development of accessible, scalable, and efficient manufacturing routes for continuous glass fiber-reinforced thermoplastic composites. To address this gap, the present study introduces a simplified nozzle-impregnation-based dual-feed FDM method for in situ fabrication of PLA composites reinforced with continuous glass fiber. The mechanical performance of the composites is systematically evaluated as a function of fiber orientation and is supported by numerical simulations, providing new insight into structure–property relationships critical to the design of anisotropic load-bearing components produced via additive manufacturing.

In this study, a dual-feed FDM setup is employed to fabricate PLA composites reinforced with continuous glass fiber using an in-nozzle impregnation technique that avoids the need for prepreg filaments or complex post-processing. Unlike previous studies that mainly focus on carbon fiber reinforcements or rely on modified printheads, this work introduces a more accessible and scalable method for producing continuous glass fiber composites. The influence of fiber orientation on tensile and flexural performance is systematically investigated and supported by finite element simulations, which show strong agreement with experimental results. This research not only bridges the gap

between traditional mold-based composite fabrication and modern additive manufacturing but also provides novel insight into anisotropic behavior and design optimization of fiber-reinforced thermoplastics for structural applications.

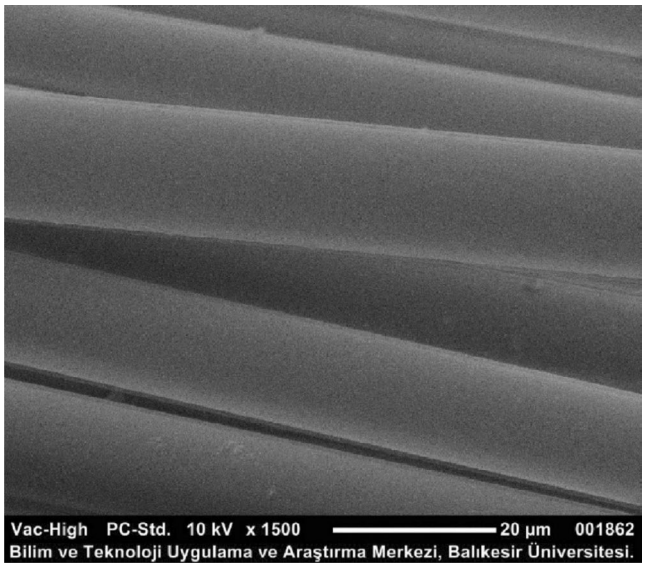

FIGURE 1 | SEM image of glass fiber.

TABLE 1 | Properties of GF and PLA.

Properties	PLA	Glass fiber
Density (g/cm^3)	1.24	2.64
Tensile strength (MPa)	20–30	2098
Elastic modulus (GPa)	3.8	76
Flexural strength (MPa)	101.2	—
Flexural modulus (GPa)	3.11	—
Filament diameter (mm)	1.75	—

2 | Materials and Methods

2.1 | Materials

In this study, continuous glass fibers (GF) (WR6 300 tex) containing 800 elementary fibers with an elementary fiber diameter of 14.75 ± 1.18 µm were used as reinforcement materials, and polylactic acid (PLA) (Esun Industrial Co. Ltd.; Shenzhen) with a filament diameter of 1.75 mm was used as the matrix material. The elementary fiber diameter of GF was determined by using ImageJ based on the image of SEM, which was shown in Figure 1. Properties of reinforcement fibers and matrix material were given in Table 1.

2.2 | 3D Printing of Continuous Glass Fiber Reinforced Composites

Continuous GF reinforced PLA composites were 3D printed by using a custom-made extruder system based on the nozzle-impregnation method. Continuous GF and PLA filaments were fed into the extruder from different inlets. Impregnation of melt PLA into the GF bundle occurred between the nozzle outlet and the fiber guide tip. A steel nozzle with a rounded tip was used to prevent nozzle wear and fiber breakage during the 3D printing process [26]. The printing temperature was fixed at 210°C, and the nozzle head speed was fixed at 10 mm/s. A schematic representation of the extruder system and an image of the 3D printing process were shown in Figure 2a,b, respectively. The line width and layer height values were fixed at 2 mm and 0.5 mm, respectively. The reinforced layer count was kept at six for all samples. Unreinforced PLA layers were deposited for the first bottom and the last top layer.

Composite specimens were 3D printed by using different infill angles to investigate the effect of fiber orientation on the properties of composites. The orientation angle of continuous GF fibers was adjusted by changing the infill angle during the slicing process. Geometric code (gcode) files, which include printing parameters such as nozzle spatial coordinates, were generated by using the slicing program [27, 28]. Fiber

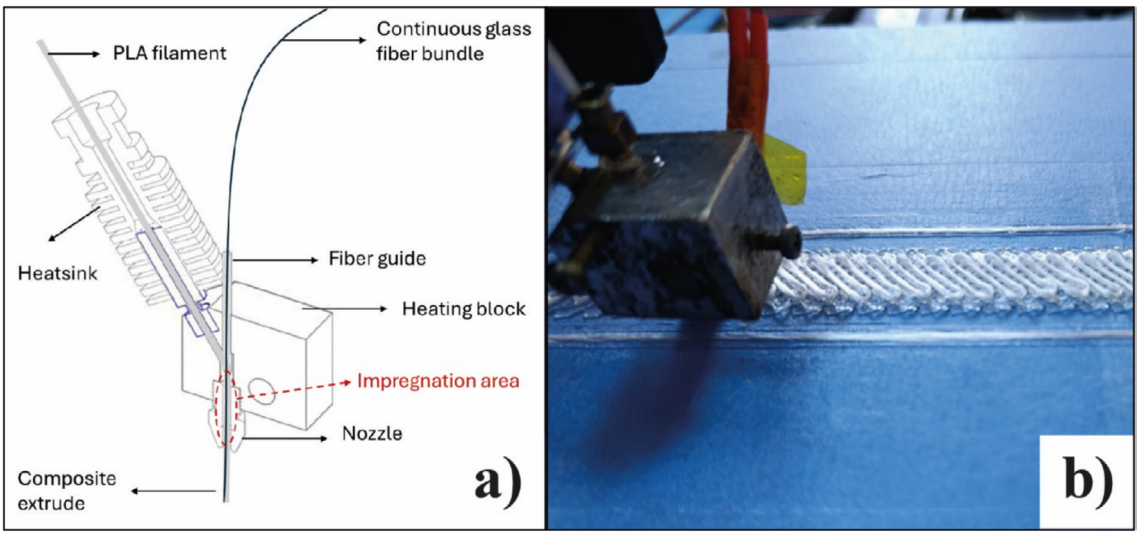

FIGURE 2 | (a) Schematic representation of extruder system and (b) image of 3D printing process.

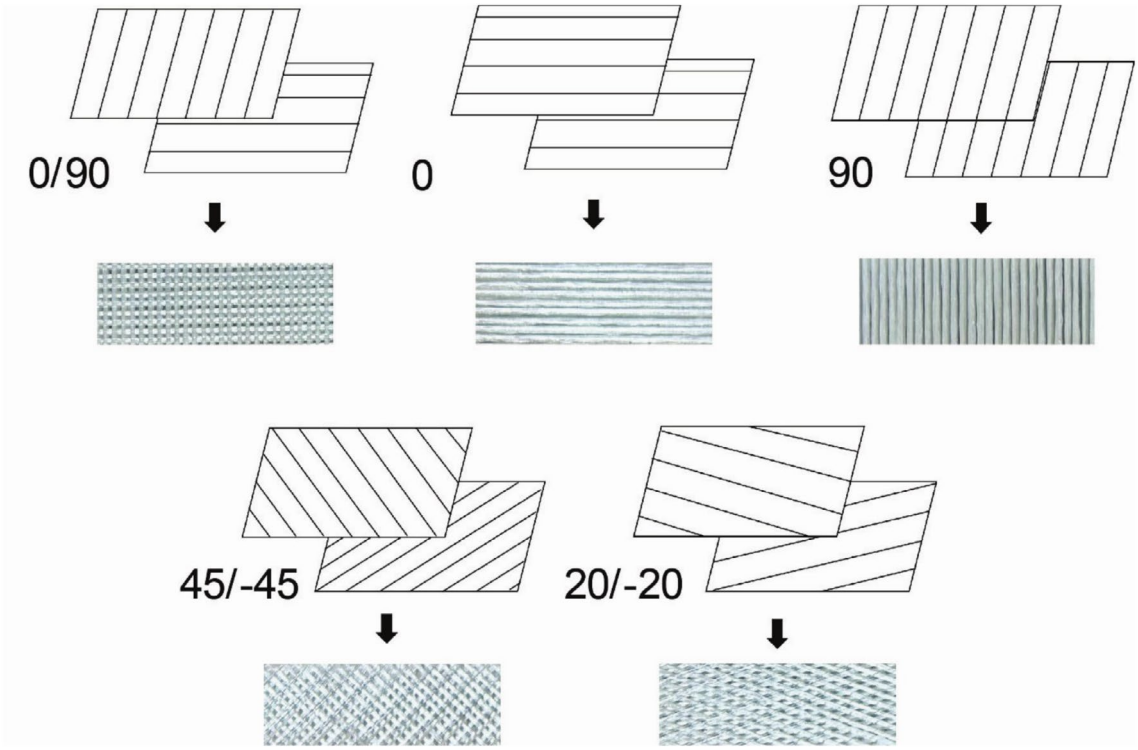

FIGURE 3 | Fiber orientation angle and patterns of composites.

orientation angle and patterns of composites were given in Figure 3.

2.3 | Characterization

Thermal behavior of PLA matrix and composite containing continuous glass fiber was investigated by thermogravimetric analyzer (TGA). TGA tests were performed by heating specimens from room temperature to 600°C with a heating rate of 10°C/min under nitrogen atmosphere. Differential scanning calorimetry (DSC) analysis was performed by using DSC analyzer (TA Instruments/DSC 250) from 30°C to 200°C with a heating ramp of 10°C/min under nitrogen atmosphere. Fiber content of composites was determined by using ignition loss method. At least 3 g of specimens were placed in alumina crucibles for each orientation parameter, and ignition process was carried out by using electrical furnace (Protherm PLF 110/30). Crucibles were heated from room temperature to 450°C with a heating rate of 10°C/min and kept at peak temperature for 1 h to ensure decomposition of PLA matrix. Volume fractions of composites were determined by the following equation [29].

$$V_f = \frac{m_{final} - m_{crucible}}{\left(m_{final} - m_{crucible}\right) + \frac{\rho_{fiber}}{\rho_{matrix}}\left(m_{initial} - m_{final}\right)} \quad (1)$$

where $m_{initinal}$, m_{final}, $m_{crucible}$, ρ_{fiber}, and ρ_{matrix} correspond to the mass of the sample before ignition, the mass of the sample after ignition, the mass of the crucible, the density of the reinforcement, and the density of the matrix.

Specimens were cut and molded by using epoxy resin for optical microscope examinations. Samples were ground by using sandpapers with a grit size of 80 to 1200 subsequent to the molding process and polished with polishing paste containing abrasive particles with a particle size of 6 μm. Scanning electron microscope (JEOL JSM-5000 NEOSCOPE) was used for the investigation of both the pristine GF morphology and the fracture surface of composites 3D printed with different fiber orientations. Specimens were machined to dimensions of 100 mm*20 mm (x*y) by using a water jet cutting system for mechanical testing. Tensile and flexural properties of the 3D-printed continuous glass fiber-reinforced PLA composites were evaluated using a Zwick/Roell universal testing machine. Tensile tests were performed in accordance with the ASTM D3039 standard, while three-point bending tests were conducted following ASTM D790. Unidirectional specimens with dimensions of 100 × 20 × 4 mm (x × y × z) were printed for tensile testing. Then, 3D-printed tabs were attached at both ends of the specimen to provide better load transfer and reduce stress concentrations at the grips. The crosshead speed for both tests was fixed at 2 mm/min. Specimen dimensions were prepared in compliance with the respective standards to ensure consistent stress distribution and valid comparison of mechanical performance across different fiber orientations. 3D printed end tabs were adhesively mounted onto tensile testing specimens before testing. Flexural strength of composites was determined by three-point bending testing with a span to depth ratio of 16 and a crosshead speed of 2 mm/min. Mechanical test samples are shown in Figure 4.

2.4 | Finite Element Modeling

In this study, a representative volume element (RVE)-based numerical modeling approach was employed to investigate the

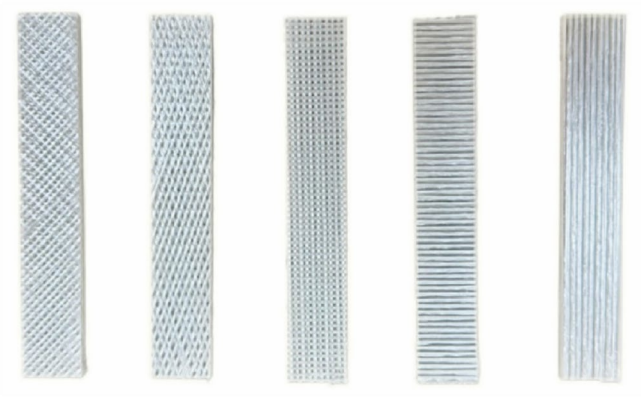

FIGURE 4 | Mechanical test samples with varying fiber orientations.

mechanical behavior of fiber-reinforced composites produced via fused deposition modeling (FDM). Unlike conventional manufacturing methods, FDM-based production often results in relatively low fiber volume fractions, which significantly limits the strength and stiffness of the final composite parts.

To overcome this limitation and to explore optimization strategies, finite element simulations were performed on idealized RVE models. These models allow us to predict the effective mechanical response of the composite by varying key microstructural parameters such as fiber volume fraction and fiber diameter. By applying appropriate boundary conditions and loading scenarios, we calculated the homogenized stiffness values and evaluated how different reinforcement configurations influence overall strength. It should be noted that the RVE models in this study were constructed using idealized fiber arrangements rather than microstructure-based reconstructions. Although SEM imaging was performed to evaluate impregnation quality, the fiber geometry in the simulations was not directly extracted from images. Instead, fiber diameter and volume fraction were determined experimentally and from printing parameters, enabling accurate input definitions. This approach ensures consistency between the fabricated and simulated composites, particularly given the precise control offered by the dual-feed additive manufacturing process. Also, the fiber–matrix interface was assumed to be perfectly bonded. This simplification was considered appropriate since the simulations were limited to the elastic regime, where interfacial failure mechanisms are not dominant.

The theoretical results and formulation of the RVE homogenization methodology were detailed in the previous work [30], and are therefore not repeated here. The RVE represents a statistically meaningful microstructural segment of the composite, consisting of reinforcing fibers embedded in a matrix phase. It is assumed that this microstructure can reflect the overall material response when subjected to mechanical loading. The fiber–matrix interactions, including mismatch in stiffness and induced internal stresses, are captured numerically using the finite element method (FEM). The mesh structure image of the unidirectional fiber composite RVE model is shown in Figure 5.

The homogenization procedure involves applying appropriate boundary conditions to the RVE and computing the average

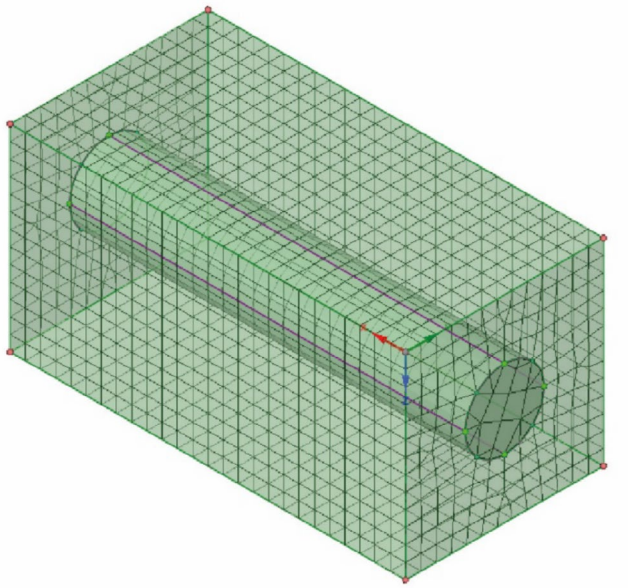

FIGURE 5 | Mesh structure of unidirectional fiber composite RVE model.

stress and strain fields under controlled loading scenarios. This allows the extraction of the effective elastic constants of the composite. The influence of fiber orientation, volume fraction, and geometric arrangement is inherently considered in this modeling framework.

The RVE models were constructed based on idealized geometric representations of the fiber architecture and meshed for numerical simulation. By evaluating the macroscopic response of the RVE, the composite's effective stiffness characteristics were determined.

3 | Results and Discussion

3.1 | Thermogravimetric (TGA) and Differential Scanning Calorimetry (DSC) Analyzes

Thermal behavior of unreinforced PLA and continuous GF composite was examined using thermogravimetric analysis (TGA), and derivative thermogravimetry (DTG) and it is shown in Figure 6a,b, respectively. According to the TGA results, unreinforced PLA exhibits thermal stability up to approximately 296°C. Beyond this point, a marked mass loss occurred, which corresponds to the degradation of the polymer. This behavior is indicative of a single-step thermal decomposition, typical of polymers with relatively uniform molecular structures. Similar single-step thermal decomposition was observed for the continuous GF composite, and incorporation of GF into the PLA matrix caused slight shifting of decomposition start temperature to lower temperatures of 292°C. The observations revealed that no improvement was observed with the incorporation of glass fiber into the polymer. The thermal degradations of specimens nearly continued up to a temperature of about 395°C. The DTG curves further support these observations by exhibiting a single, prominent

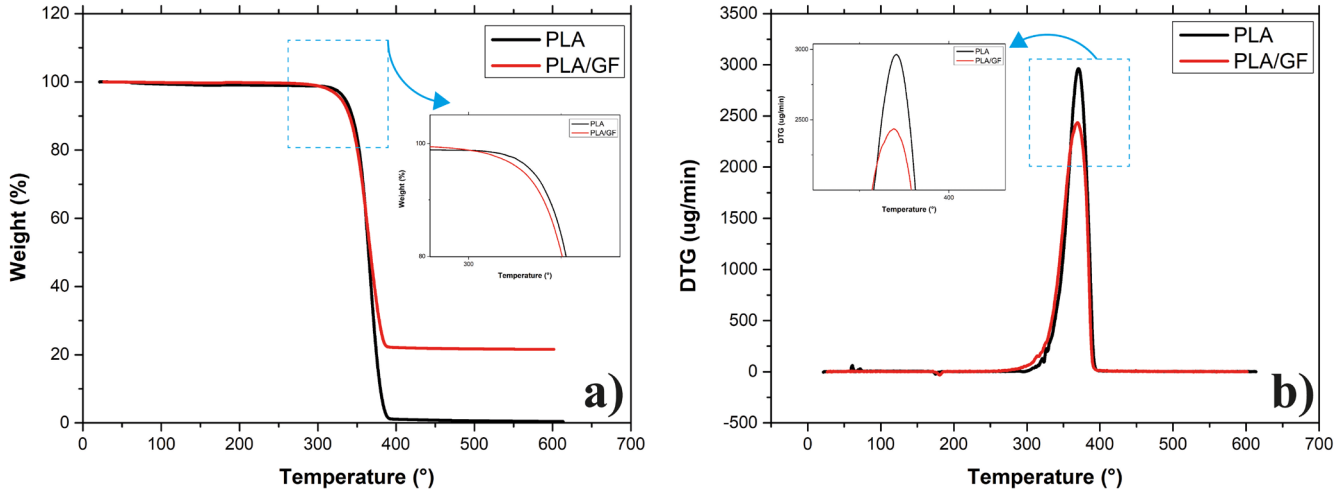

FIGURE 6 | (a) TGA and (b) DTG curves of unreinforced PLA and continuous GF composite.

peak corresponding to the maximum rate of mass loss at 370.61°C and 369.08°C for unreinforced polymer and the composite, respectively. Remaining mass loss values were 0.39% and 21.55% for unreinforced and continuous GF composite. Results confirm that the degradation of PLA and the composite occurs primarily in a single step under the applied thermal conditions [31]. The slight decrease in the onset degradation temperature was observed. Pathek et al. [32] indicated that the presence of fibers in the composites can act as initiation points for thermal degradation due to weak interfacial interactions.

DSC analysis of pure PLA and its composites indicated the occurrence of both heat-absorbing (endothermic) and heat-releasing (exothermic) transitions during analysis. The initial thermal peak for neat PLA, detected at 62.1°C, corresponds to the glass transition temperature, aligning with findings reported by Chen et al. [33]. A subsequent exothermic peak at 96.58°C signifies the occurrence of cold crystallization. Furthermore, a smaller exothermic peak at 163.43°C is linked to melt-induced crystallization [34]. The final endothermic peak, appearing at 180.65°C, is associated with the melting point of the PLA polymer matrix [35]. The incorporation of glass fibers led to a discernible decrease in the intensity of the thermal peaks, indicating an influence on the crystallization and melting behavior of the composite. The glass transition, cold crystallization, and melting peaks were determined as 62.9°C, 95.88°C, and 179.59°C, respectively. Because the fibers were too macroscopic to affect the mobility of the polymer chain segments and weak interfacial interactions, a slight decrease in the crystallization and melting points was observed [32, 36]. DSC thermograms of neat PLA and composite are presented in Figure 7 to compare their thermal transitions.

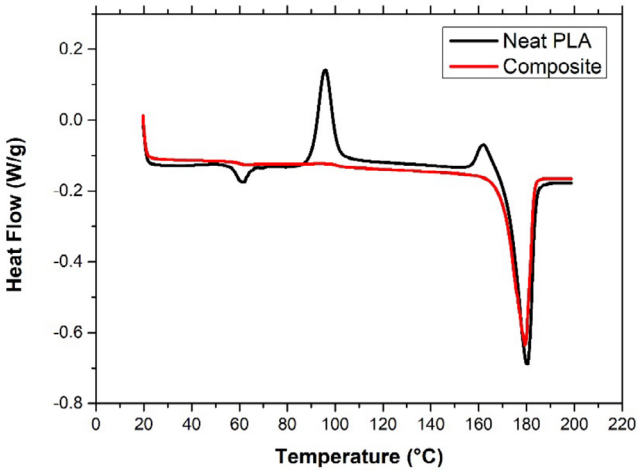

FIGURE 7 | DSC analysis of neat PLA and composite.

3.2 | Optical Microscope Investigation Results

Optical microscope images of 3D printed continuous GF reinforced composites with fiber orientations of 0° and 90° were shown in Figure 8 a and b respectively. As expected, fibers were vertically and horizontally located for 0° and 90°, respectively. The existence of pores derived from the poor impregnation of polymer into the bundles of fibers was clearly observed. Due to the increased ratio of nozzle diameter to layer height and nozzle force applied onto fibers during the printing process, the cross-sectional geometry of fiber bundles tended to be elliptical [37].

3.3 | Fiber Content of Composites

Volume fractions of composites 3D printed with various fiber orientations were determined by using the ignition loss approach. The calculations (see Equation 1) were based on the ignition loss of composites at 450°C for 1 h. The temperature was selected based on the TGA analysis, where no further mass change was observed. The mass loss of the composites originated from the decomposition of matrix PLA, and the result indicated the presence of reinforcing fibers GF. The fiber content of 3D printed continuous GF composites was determined to be ~12.5 vol.%, and the variation of fiber orientation caused no obvious change in fraction results due to the fixed parameters of linewidth and layer height. It was indicated in the literature that the decrease in both linewidth and layer height results in an increase in the fiber content of the composites [7, 25, 26]. Fiber volume fractions for each orientation are given in Table 2.

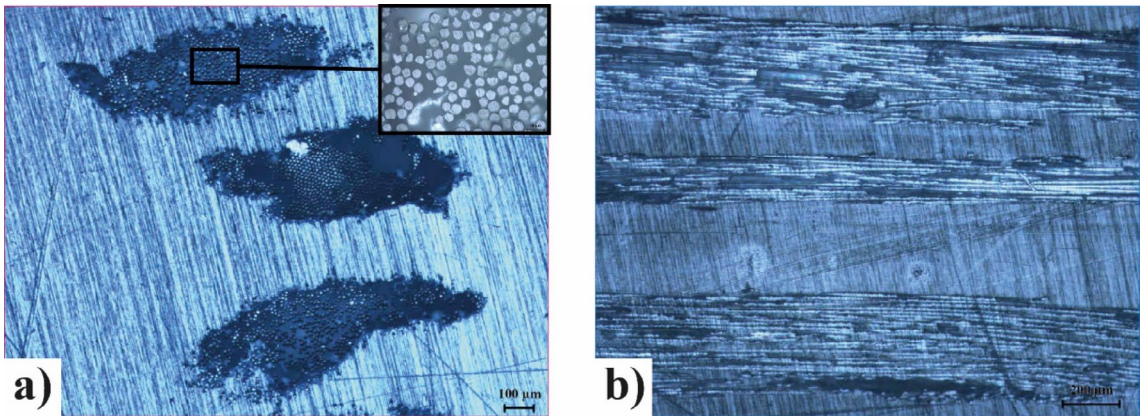

FIGURE 8 | Optical microscope images of composites with fiber orientations of (a) 0° and (b) 90°.

TABLE 2 | Fiber volume fraction (vol.%) for each orientation.

Fiber orientation	Fiber volume fraction
0	12.46 ± 0.5
90	12.37 ± 1.8
0/90	12.61 ± 0.7
45/−45	12.48 ± 0.5
20/−20	12.55 ± 1.1

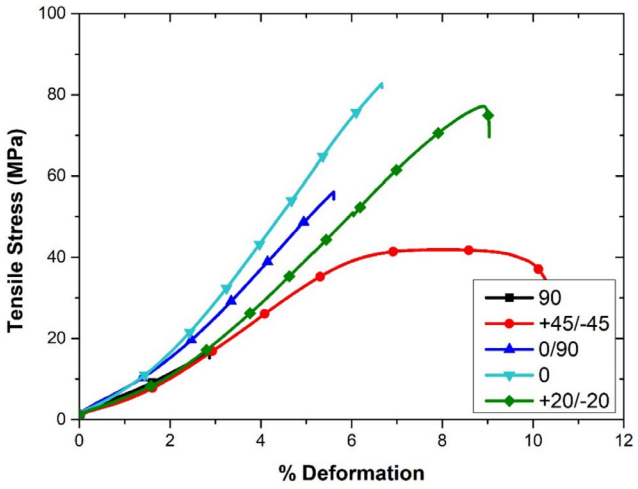

FIGURE 9 | Tensile stress of glass fiber-reinforced PLA composites as a function of fiber orientation.

3.4 | Tensile and Bending Test

The influence of fiber orientation on the tensile performance of continuous glass fiber-reinforced PLA composites was systematically investigated. Tensile strength values obtained for different orientations are presented in Figure 9. The elastic modulus values reported in this study were determined from the slope of the initial linear region of the stress–strain curves obtained during tensile testing. These curves provide a direct measure of stiffness for each fiber orientation.

The mechanical performance of the 3D-printed continuous glass fiber-reinforced PLA composites was found to be highly sensitive to fiber orientation. The specimen with 0° fiber alignment exhibited the highest tensile strength of 82.75 MPa and a corresponding elastic modulus of 13.36 GPa, confirming that direct axial alignment facilitates optimal load transfer and stiffness. This result is consistent with classical composite theory and prior studies [38–41], where reinforcement along the loading direction maximizes both strength and modulus.

Specimens printed with ±20° orientation achieved a relatively high tensile strength of 77.18 MPa and an elastic modulus of 9.48 GPa, indicating that near-axial fibers can still effectively bridge microcracks and distribute stress. The 0/90° cross-ply configuration provided moderate values (56.08 MPa, 10.20 GPa), where longitudinal fibers contributed to strength while transverse fibers acted primarily as stabilizers.

As expected, the ±45° orientation resulted in reduced performance due to off-axis fiber alignment and shear-dominated failure modes, with tensile strength and modulus measured as 41.86 MPa and 6.89 GPa, respectively. In off-axis configurations such as ±20° and ±45°, no signs of delamination or out-of-plane failure were observed. The failure was primarily due to fiber pull-out, resulting from poor impregnation. The 90° configuration, where fibers are perpendicular to the loading direction, showed the weakest performance: 16.21 MPa tensile strength and 5.16 GPa elastic modulus. This behavior is attributed to matrix-dominated failure mechanisms, including interfacial debonding and fiber pull-out, as the load is primarily borne by the PLA matrix.

These findings align with simulation-based and experimental results in the literature [39, 40, 42], all of which emphasize the critical influence of fiber orientation on the tensile response of both synthetic and natural fiber-reinforced composites.

The bending performance of the continuous glass fiber-reinforced PLA composites produced via additive manufacturing (AM) exhibited a pronounced dependence on fiber orientation. Figure 10. Effect of fiber orientation on the flexural strength of 3D-printed continuous glass fiber-reinforced PLA composites. The 0° orientation exhibited the highest flexural strength due to optimal fiber alignment with the principal stress

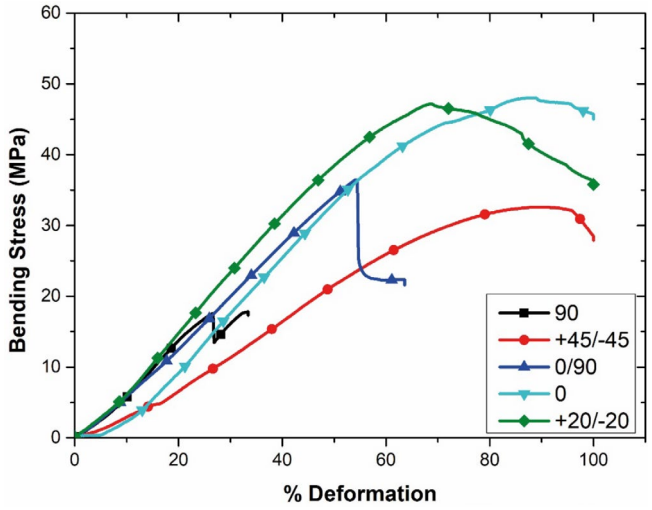

FIGURE 10 | Bending stress of glass fiber-reinforced PLA composites as a function of fiber orientation.

direction, whereas off-axis configurations such as ±45° and 90° resulted in significantly reduced performance due to ineffective stress transfer and matrix-dominated failure. Among all tested configurations, the specimen printed with 0° fiber alignment showed the highest flexural strength (48.04 MPa), benefiting from optimal reinforcement alignment along the principal tensile stress direction during bending. A similarly high flexural strength was observed in the ±20° configuration (47.16 MPa), indicating that small deviations from the loading axis can still effectively contribute to load-bearing through fiber bridging mechanisms and distributed stress absorption.

The 0/90° cross-ply configuration yielded an intermediate strength (36.42 MPa), reflecting a balance between longitudinal reinforcement and transverse structural support. In contrast, the ±45° orientation (32.60 MPa) resulted in lower flexural strength due to shear-induced deformation and reduced axial stiffness. The lowest flexural strength was recorded in the 90° configuration (17.81 MPa), where fibers were oriented perpendicular to the bending axis, thus failing to contribute meaningfully to tensile resistance on the outermost fiber layer.

The flexural test results of the continuous glass fiber-reinforced PLA composites revealed that fiber orientation has a decisive influence on bending performance. Specimens with 0° fiber alignment exhibited the highest bending strength, as the fibers are optimally positioned to carry both tensile and compressive loads along the bending axis. Consistent with the results of Baharlou et al. [43], the present study confirms that 0° fiber orientation provides superior flexural strength among all tested configurations due to its favorable alignment with the principal stress directions during bending. As the fiber orientation deviated from the loading direction—such as in the ±45° and 90° configurations—mechanical performance declined considerably. A similar trend was reported by Singh et al. [44], who observed that the flexural strength of symmetric glass/epoxy laminates decreased by up to 36.07% in 45°-oriented specimens compared to those with 0° orientation. These reductions are consistent with the strength losses found in the off-axis specimens of the present study. Furthermore, the current findings are in agreement with Wang et al. [45], who showed that increased layer height and extrusion width in FDM printing result in a broader distribution of fiber orientations, which can in some cases enhance resistance to bending loads by promoting more isotropic reinforcement behavior—particularly relevant in short fiber-reinforced composites.

3.5 | Scanning Electron Microscope (SEM)

SEM micrographs of 3D printed continuous GF reinforced PLA composites with various fiber orientations are shown in Figure 11a,e for the specimens with a fiber orientation of 0° to 90°. Straight broken fibers were observed for all orientations except for the composite printed with a fiber orientation of 90° (see Figure 11e). Pore presence was obvious in the fiber bundles due to the poor impregnation. Due to the lack of effective impregnation of PLA melt into GF bundles during extrusion, fibers located perpendicular to the applied tensile load were peeled off and scattered from the PLA matrix. The poor impregnation of polymer melt into fiber bundles was observed in studies based on the nozzle-impregnation method due to the presence of a limited impregnation area in the hot-end system which can be eliminated by the use of pre-impregnated fiber bundles [46–48]. Similarly, no failure based on fiber breakage was observed in specimens printed at a 90° orientation. In this orientation, failure originated from the separation at the fiber-matrix interface. As the orientation angle approached 90°, the fracture behavior resulted in both matrix and fiber failure due to the load transmitted to the fibers. The common point for the failure behavior for fibers subjected to tensile load was fiber breakage and pull-out of fibers from the PLA matrix due to the weak interaction between the fiber-matrix interface. Due to this weak interaction between the fiber-matrix and the smooth surface profile of fibers, no PLA matrix residue was observed on the surface of fractured fibers during examinations. A representative SEM image illustrating fiber pull-out, voids, and interfacial gaps is also shown in Figure 12.

3.6 | Finite Element Results

Finite element analysis (FEA) was conducted to investigate the effect of fiber orientation and volume fraction on the elastic modulus of 3D-printed continuous glass fiber-reinforced PLA composites. The RVE simulations were used to extract orthotropic elastic properties of the unidirectional composite lamina. Since the specimens were cut from flat printed plates, the material behaves similarly to conventionally manufactured laminates. Off-axis properties can therefore be derived using classical lamination theory by inputting the calculated 0° and 90° moduli, without the need for additional angle-specific simulations. Thus, simulations were performed for two primary fiber orientations: 0° and 90°.

The FEA results revealed an elastic modulus of 12,893 MPa for the 0° orientation and 5185 MPa for the 90° orientation. These values are in good agreement with the experimental measurements, which yielded 13,357 MPa and 5160 MPa, respectively. The close match between numerical and experimental results supports the validity of the RVE-based simulation approach and

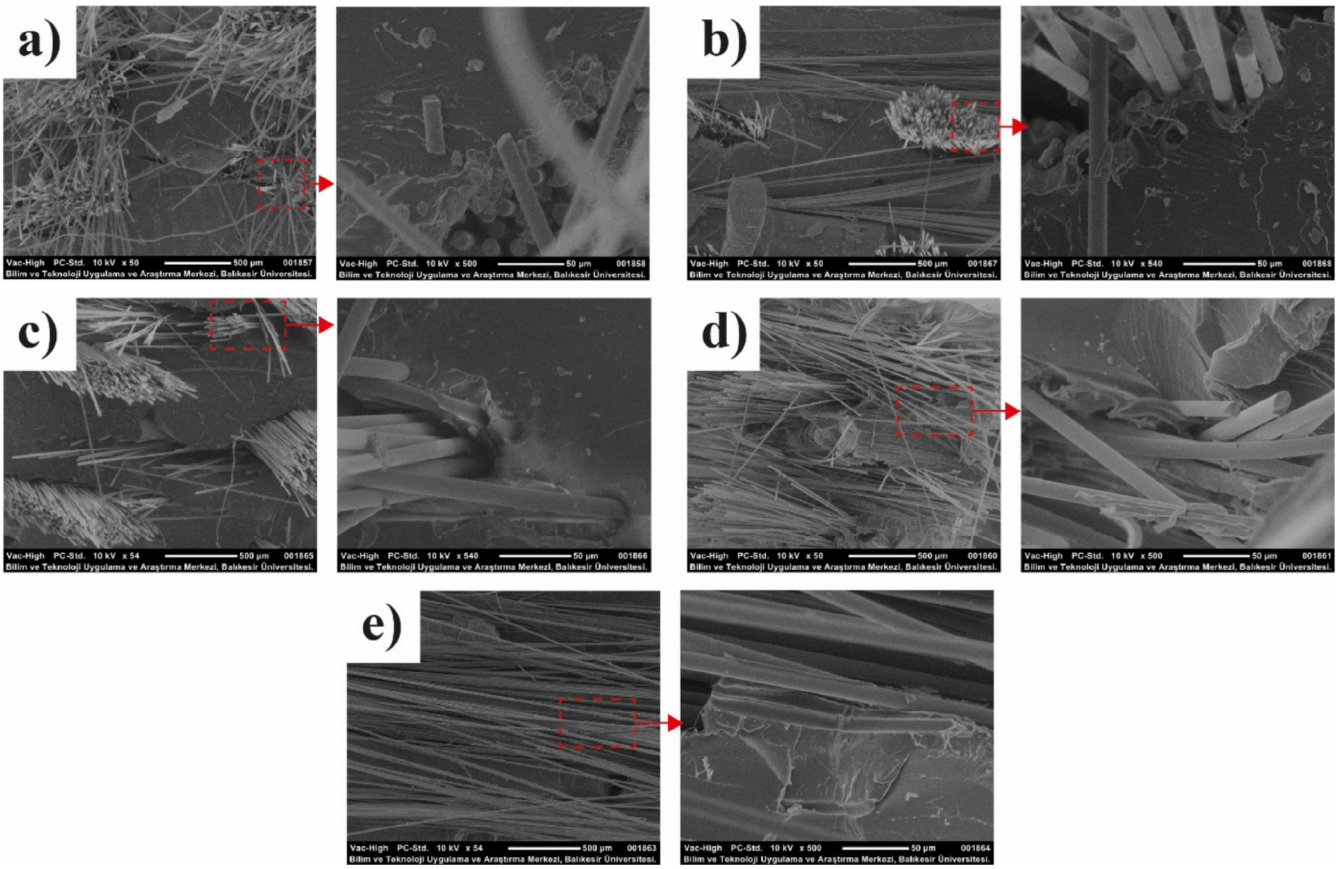

FIGURE 11 | Fracture surface SEM images of composites 3D printed with fiber orientations of (a) 0, (b) 0/90, (c) +45/−45, (d) +20/−20, and (e) 90.

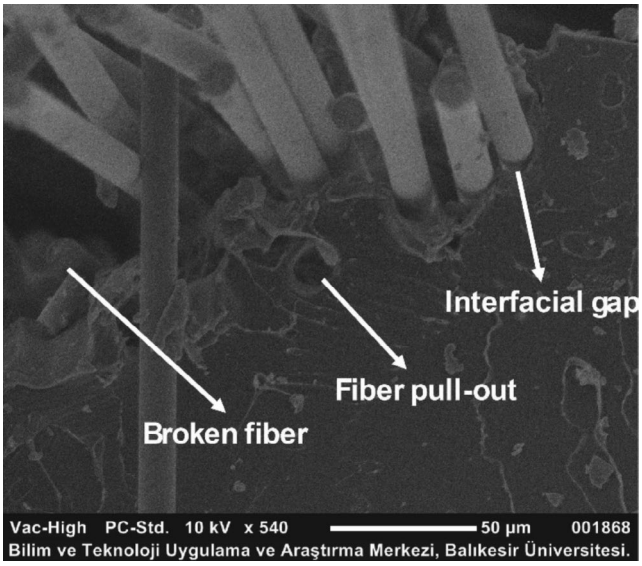

FIGURE 12 | SEM image showing fiber pull-out, voids, and interfacial gaps.

suggests that the assumed fiber distribution and interface behavior in the model are reasonably accurate.

In addition to the fixed-orientation simulations, a parametric study was conducted to evaluate how changes in fiber volume fraction (ranging from 8% to 20%) affect the elastic properties of the composite. As shown in Figure 13, stiffness in the 0° fiber orientation direction increased nonlinearly with fiber content, indicating improved load-bearing capability along the fiber axis as reinforcement increased. Meanwhile, stiffness in the 90° orientation—perpendicular to the loading direction—also showed a gradual increase, albeit to a lesser extent. These trends confirm the anisotropic nature of the material, where the mechanical response is highly dependent on fiber alignment relative to the applied load.

These results collectively highlight the critical role of fiber alignment and volume fraction in tailoring the mechanical behavior of additively manufactured composites. The parametric FEA outcomes also provide valuable guidelines for optimizing process parameters to meet specific stiffness requirements.

To better contextualize the current study, a comparative summary of recent works on continuous fiber-reinforced thermoplastic composites is presented in Table 3. The table highlights differences in reinforcement type, matrix material, fabrication method, and mechanical performance across studies. This comparison emphasizes the originality and performance advantages of the present work, particularly in terms of the use of a simplified dual-feed FDM process and fiber alignment control.

4 | Conclusion

In this study, continuous glass fiber-reinforced PLA composites were successfully fabricated using a dual-feed fused deposition

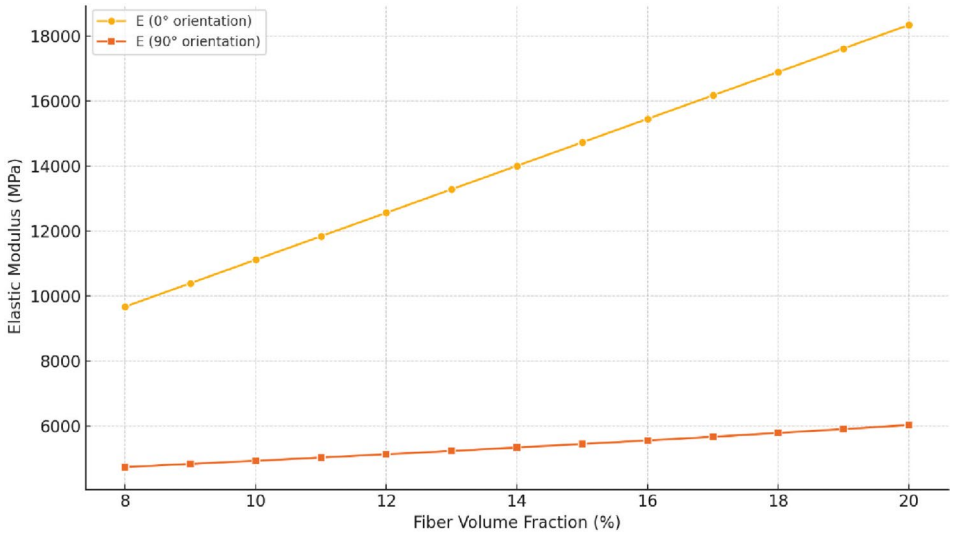

FIGURE 13 | Effect of fiber volume fraction on elastic modulus for 0° and 90° orientations.

TABLE 3 | Comparative summary of recent studies on continuous fiber-reinforced thermoplastic composites and the present work.

Matrix	Fiber content	Fiber orientation	Tensile strength (MPa)	References
PLA	45 wt.%	0	241	[49]
PLA	60 vol.%	0	345.74	[50]
Nylon	8 vol.%	0	73.35	[50]
Nylon	15 vol.%	0	139	[21]
Nylon	75 vol.%	0	272	[21]
Nylon	15 vol.%	45	116	[21]
Nylon	75 vol.%	45	159	[21]
PA6	5.6 vol.%	0	115.2 ± 16.5	[51]
PA6	17.1 vol.%	0	218.2 ± 2.9	[51]
PLA	23 vol.%	0	139.64 ± 6.2	[52]
PLA	12.46 ± 0.5	0	82.75	This work
PLA	12.37 ± 1.8	90	16.21	This work
PLA	12.61 ± 0.7	0/90	56.08	This work
PLA	12.48 ± 0.5	45/−45	41.86	This work
PLA	12.55 ± 1.1	20/−20	77.18	This work

modeling (FDM) system based on the nozzle-impregnation method, with a specific focus on the influence of fiber orientation on mechanical performance. A consistent fiber volume fraction of approximately 12.5 vol.% was confirmed for all samples via ignition loss analysis, enabling a reliable comparison across orientation configurations. Thermogravimetric analysis (TGA) revealed that the incorporation of glass fibers slightly reduced the onset degradation temperature of PLA, while maintaining its single-step decomposition behavior.

Mechanical testing showed that specimens with 0° fiber alignment achieved the highest tensile and flexural strengths of 82.75 MPa and 48.04 MPa, respectively, which were approximately 5.1 and 2.7 times higher than those of the 90° orientation (16.21 MPa and 17.81 MPa). Similarly, the 0° configuration yielded an elastic modulus of 13.36 GPa—about 2.6 times greater than the 5.16 GPa recorded for the 90° orientation—indicating pronounced anisotropy resulting from directional reinforcement.

Fractographic analysis by SEM revealed clear signs of fiber pull-out and interfacial debonding in off-axis samples, particularly at 90°, confirming ineffective load transfer due to insufficient wetting of glass fibers by the PLA matrix. These findings reflect a typical limitation of nozzle-based in situ impregnation systems.

Finite element analysis using representative volume elements (RVEs) closely matched experimental elastic modulus values and further demonstrated that increasing the fiber volume fraction significantly enhances stiffness along the fiber direction. These results collectively validate the mechanical trends and provide valuable design guidelines for tuning stiffness and strength in continuous fiber-reinforced thermoplastics.

Overall, this study highlights the dominant role of fiber alignment in dictating the tensile and bending behavior of continuous glass fiber-reinforced PLA composites produced via additive manufacturing. The quantitative insights derived herein strengthen the understanding of structure–property relationships and underscore the importance of precise fiber path control in achieving tailored anisotropic performance.

Author Contributions

Ahmet Cagri Kilinc: writing – original draft, writing – review and editing, methodology, conceptualization, investigation. **Turker Turkoglu:** conceptualization, investigation, writing – original draft, methodology. **Volkan Arikan:** software, writing – original draft, writing – review and editing. **Sare Celik:** writing – review and editing, supervision. **Fidan Bilir Kilinc:** writing – original draft, conceptualization. **Selcuk Yesiltepe:** conceptualization, investigation, writing – original draft.

Acknowledgments

The authors thank Türkiye Şişe ve Cam Fabrikaları A.Ş and BAKOMER (Balıkesir University Composite Research Training-Simulation Application and Research Center) for their support.

Conflicts of Interest

The authors declare no conflicts of interest.

Data Availability Statement

The data that support the findings of this study are available from the corresponding author upon reasonable request.

References

1. T. Mengesha Medibew, "A Comprehensive Review on the Optimization of the Fused Deposition Modeling Process Parameter for Better Tensile Strength of PLA-Printed Parts," *Advances in Materials Science and Engineering* 2022 (2022): 1–11, https://doi.org/10.1155/2022/5490831.

2. P. Cheng, Y. Peng, S. Li, et al., "3D Printed Continuous Fiber Reinforced Composite Lightweight Structures: A Review and Outlook," *Composites. Part B, Engineering* 250, no. November 2022 (2023): 110450, https://doi.org/10.1016/j.compositesb.2022.110450.

3. Y. Gür, S. Çelik, and R. Sakin, "Tensile Behaviour of Continuous Carbon Fibre Reinforced Composites Fabricated by a Modified 3D Printer," *Materials Research Express* 11, no. 7 (2024): 075305, https://doi.org/10.1088/2053-1591/ad62c0.

4. M. Khosroupour Arabi and N. Kordani, "3D-Printing of Continuous Fiber: A Review of Processes, Materials and Properties," *Polymer Technology and Materials* 62, no. 12 (2023): 1525–1559, https://doi.org/10.1080/25740881.2023.2222793.

5. A. Thirugnanasamabandam, M. Subramaniyan, B. Prabhu, and K. Ramachandran, "Development and Comprehensive Investigation on PLA / Carbon Fiber Reinforced PLA Based Structurally Alternate Layered Polymer Composites," *Journal of Industrial and Engineering Chemistry* 136, no. February (2024): 248–257, https://doi.org/10.1016/j.jiec.2024.02.012.

6. F. Safari, A. Kami, and V. Abedini, "3D Printing of Continuous Fiber Reinforced Composites: A Review of the Processing, Pre- and Post-Processing Effects on Mechanical Properties," *Polymers and Polymer Composites* 30 (2022): 30, https://doi.org/10.1177/09673911221098734.

7. T. Turkoglu and A. C. Kilinc, "Optimization of Process Parameters for Steel Wire-Reinforced Polylactic Acid Composites Produced by Additive Manufacturing," *Polymers* 17, no. 5 (2025): 624, https://doi.org/10.3390/polym17050624.

8. V. Gavande and A. Anand, "On the Mechanical Properties of Continuous Fiber Reinforced Thermoplastic Composites Realized Through Vacuum Infusion," *Journal of Composite Materials* 54, no. 27 (2020): 4231–4239, https://doi.org/10.1177/0021998320928120.

9. D. Hoagland and A. George, "Continuous Permeability Measurement During Unidirectional Vacuum Infusion Processing," *Journal of Reinforced Plastics and Composites* 36, no. 22 (2017): 1618–1628, https://doi.org/10.1177/0731684417721660.

10. X. Liu, Y. Cao, C. Zhang, et al., "Study on Mechanical Properties of Vacuum-Infused Glass Fiber Reinforced Thermoplastic Methacrylic Resin Composites," *Polymer Composites* 45, no. 8 (2024): 7024–7038, https://doi.org/10.1002/pc.28245.

11. A. Agirregomezkorta, M. Sánchez-Soto, G. Aretxaga, M. Sarrionandia, and J. Aurrekoetxea, "Effects of Vacuum Infusion Processing Parameters on the Impact Behavior of Carbon Fiber Reinforced Cyclic Butylene Terephthalate Composites," *Journal of Composite Materials* 48, no. 3 (2014): 333–344, https://doi.org/10.1177/0021998312472218.

12. E. Pizzi and F. Trovalusci, "Manufacturing by Resin Infusion and Characterization of Hybrid Carbon/Glass Fiber–Reinforced Plastic From Recycled Carbon Fiber," *International Journal of Advanced Manufacturing Technology* 137, no. 1–2 (2025): 619–631, https://doi.org/10.1007/s00170-025-15233-3.

13. S. Olhan and B. K. Behera, "Development of GNP Nanofiller Based Textile Structural Composites for Enhanced Mechanical, Thermal, and Viscoelastic Properties for Automotive Components," *Advanced Composites and Hybrid Materials* 7, no. 1 (2024): 25, https://doi.org/10.1007/s42114-024-00834-5.

14. S. Olhan, B. Antil, and B. K. Behera, "Repair Technologies for Structural Polymeric Composites: An Automotive Perspective," *Composite Structures* 352 (2025): 118711, https://doi.org/10.1016/j.compstruct.2024.118711.

15. S. Olhan and B. K. Behera, "Mechanical, Thermogravimetric, and Dynamic Mechanical Behavior of High-Performance Textile Structural Composite Panels for Automotive Applications," *Journal of Manufacturing Processes* 102, no. August (2023): 608–621, https://doi.org/10.1016/j.jmapro.2023.08.003.

16. S. Olhan, B. Antil, and B. K. Behera, "Progress in Metal Additive Manufacturing Using Innovative Solid-State Friction Stir-Based Techniques," *Journal of Alloys and Compounds* 1010, no. September 2024 (2025): 177395, https://doi.org/10.1016/j.jallcom.2024.177395.

17. S. Olhan, B. Antil, and B. K. Behera, "Low-Velocity Impact and Quasi-Static Post-Impact Compression Analysis of Woven Structural Composites for Automotive: Influence of Fibre Types and Architectural Structures," *Composite Structures* 352, no. October 2024 (2025): 118676, https://doi.org/10.1016/j.compstruct.2024.118676.

18. S. S. Luke, D. Soares, J. V. Marshall, J. Sheddden, and Ö. Keleş, "Effect of Fiber Content and Fiber Orientation on Mechanical Behavior of Fused Filament Fabricated Continuous-Glass-Fiber-Reinforced Nylon," *Rapid Prototyping Journal* 27, no. 7 (2021): 1346–1354, https://doi.org/10.1108/RPJ-01-2021-0003.

19. M. Naik, D. Thakur, and S. Salunkhe, "Evaluation of Thermal and Mechanical Properties of Continuous Fiberglass Reinforced Thermoplastic Composite Fabricated by Fused Deposition Modeling," *Journal*

of Applied Polymer Science 140, no. 26 (2023): 1–11, https://doi.org/10.1002/app.53989.

20. N. Mosleh, S. Dariushi, and M. Esfandeh, "An Experimental and Numerical Investigation on Mechanical Properties of 3D Printed Continuous Glass Tow Preg-Reinforced Composites," *Rapid Prototyping Journal* 28, no. 7 (2022): 1284–1296, https://doi.org/10.1108/RPJ-08-2021-0200.

21. M. R. Khosravani, P. Frohn-Sörensen, J. Reuter, B. Engel, and T. Reinicke, "Fracture Studies of 3D-Printed Continuous Glass Fiber Reinforced Composites," *Theoretical and Applied Fracture Mechanics* 119, no. February (2022): 103317, https://doi.org/10.1016/j.tafmec.2022.103317.

22. C. Dong and I. J. Davies, "Mechanical Properties of Continuous Glass Fibre-Reinforced Composites Made by Material Extrusion," *Progress in Additive Manufacturing* 9, no. 6 (2024): 2131–2141, https://doi.org/10.1007/s40964-024-00566-4.

23. K. M. M. Billah, F. A. R. Lorenzana, N. L. Martinez, R. B. Wicker, and D. Espalin, "Thermomechanical Characterization of Short Carbon Fiber and Short Glass Fiber-Reinforced ABS Used in Large Format Additive Manufacturing," *Additive Manufacturing* 35, no. May (2020): 101299, https://doi.org/10.1016/j.addma.2020.101299.

24. H. Dou, Y. Cheng, W. Ye, et al., "Effect of Process Parameters on Tensile Mechanical Properties of 3D Printing Continuous Carbon Fiber-Reinforced PLA Composites," *Materials (Basel)* 13, no. 17 (2020): 3850, https://doi.org/10.3390/ma13173850.

25. F. B. Kilinc, E. Bozaci, A. C. Kilinc, and T. Turkoglu, "Effect of Atmospheric Plasma Treatment on Mechanical Properties of 3D-Printed Continuous Aramid Fiber/PLA Composites," *Polymers (Basel)* 17, no. 3 (2025): 397, https://doi.org/10.3390/polym17030397.

26. F. B. Kilinc, T. Turkoglu, S. Guler, and A. C. Kilinc, "Optimization of 3D Printing Parameters for Enhanced Tensile Properties in Continuous Carbon Fiber Reinforced PLA Composites," *Materials Research Express* 12, no. 4 (2025): 045302, https://doi.org/10.1088/2053-1591/adc5cc.

27. B. Fan, S. Yang, L. Wang, and M. Xu, "Spatially Resolved Defect Characterization and Fidelity Assessment for Complex and Arbitrary Irregular 3D Printing Based on 3D P-OCT and GCode," *Sensors (Basel)* 24, no. 11 (2024): 3636, https://doi.org/10.3390/s24113636.

28. P. John, V. R. Komma, and S. P. Bhore, "Development of MATLAB Code for Tool Path Data Extraction From the G Code of the Fused Filament Fabrication (FFF) Parts," *Engineering Research Express* 5, no. 2 (2023): 025018, https://doi.org/10.1088/2631-8695/accc6f.

29. L. Ciprian, P. Radu, and E. Ioana, "The Effects of Fibre Volume Fraction on a Glass-Epoxy Composite Material," *INCAS Bulletin* 7, no. 3 (2015): 113–119, https://doi.org/10.13111/2066-8201.2015.7.3.10.

30. V. Arikan, "The Influence of Yarn Fiber Volume Fraction, Shear Angle, and Yarn Spacing on Crack Propagation Resistance of Plain-Woven Fabric-Reinforced Epoxy Composites," *Polymer Composites* 44, no. 9 (2023): 5608–5618, https://doi.org/10.1002/pc.27513.

31. M. B. Agustin, F. Nakatsubo, and H. Yano, "The Thermal Stability of Nanocellulose and Its Acetates With Different Degree of Polymerization," *Cellulose* 23, no. 1 (2016): 451–464, https://doi.org/10.1007/s10570-015-0813-x.

32. I. A. Pathek, J. R. F. da Silva, D. D. Lima, I. F. Limberger, A. A. Buenos, and C. J. Scheuer, "Assessment of Carbon Fiber Incorporation Effects on Overall Characteristics and Properties of 3D-Printed PLA," *Journal of the Brazilian Society of Mechanical Sciences and Engineering* 46, no. 11 (2024): 640, https://doi.org/10.1007/s40430-024-05233-x.

33. J. M. Chen, Y. Y. Tseng, D. Lee, et al., "A Robust Experimental Model to Explore the Three-Dimensional Printing of Polylactide Parts: Solution Versus Melt Extrusion," *Applied Sciences* 10, no. 2 (2020): 509, https://doi.org/10.3390/app10020509.

34. L. Suryanegara, A. N. Nakagaito, and H. Yano, "The Effect of Crystallization of PLA on the Thermal and Mechanical Properties of Microfibrillated Cellulose-Reinforced PLA Composites," *Composites Science and Technology* 69, no. 7–8 (2009): 1187–1192, https://doi.org/10.1016/j.compscitech.2009.02.022.

35. O. Mysiukiewicz and M. Barczewski, "Crystallization of Polylactide-Based Green Composites Filled With Oil-Rich Waste Fillers," *Journal of Polymer Research* 27, no. 12 (2020): 374, https://doi.org/10.1007/s10965-020-02337-5.

36. T. Klaser, L. Balen, Ž. Skoko, L. Pavić, and A. Šantić, "Polylactic Acid–Glass Fiber Composites: Structural, Thermal, and Electrical Properties," *Polymers (Basel)* 14, no. 19 (2022): 4012, https://doi.org/10.3390/polym14194012.

37. V. E. Kuznetsov, A. N. Solonin, O. D. Urzhumtsev, R. Schilling, and A. G. Tavitov, "Strength of PLA Components Fabricated With Fused Deposition Technology Using a Desktop 3D Printer as a Function of Geometrical Parameters of the Process," *Polymers (Basel)* 10, no. 3 (2018): 313, https://doi.org/10.3390/polym10030313.

38. A. Parmiggiani, M. Prato, and M. Pizzorni, "Effect of the Fiber Orientation on the Tensile and Flexural Behavior of Continuous Carbon Fiber Composites Made via Fused Filament Fabrication," *International Journal of Advanced Manufacturing Technology* 114, no. 7–8 (2021): 2085–2101, https://doi.org/10.1007/s00170-021-06997-5.

39. N. Niknafs Kermani, S. G. Advani, and J. Férec, "Orientation Predictions of Fibers Within 3D Printed Strand in Material Extrusion of Polymer Composites," *Additive Manufacturing* 77, no. September (2023): 103781, https://doi.org/10.1016/j.addma.2023.103781.

40. P. Pibulchinda, E. Barocio, A. J. Favaloro, and R. B. Pipes, "Influence of Printing Conditions on the Extrudate Shape and Fiber Orientation in Extrusion Deposition Additive Manufacturing," *Composites Part B: Engineering* 261, no. May (2023): 110793, https://doi.org/10.1016/j.compositesb.2023.110793.

41. S. Li, K. Wang, W. Zhu, Y. Peng, S. Ahzi, and F. Chinesta, "Investigation on the Mechanical Properties of 3D Printed Hybrid Continuous Fiber-Filled Composite Considering Influence of Interfaces," *International Journal of Advanced Manufacturing Technology* 123, no. 9–10 (2022): 3147–3158, https://doi.org/10.1007/s00170-022-10398-7.

42. M. R. Islam, M. F. Hossain, M. S. Rana, and M. S. Ferdous, "Effect of Fiber Orientation on Mechanical Properties of JUCO Fiber Reinforced Epoxy Composites," *Hybrid Advances* 8 (2025): 100386, https://doi.org/10.1016/j.hybadv.2025.100386.

43. E. Baharlou and J. Ma, "Effect of Raster Orientation on Large-Scale Robotic 3D Printing of Short Carbon Fiber-Reinforced PLA Composites," *Additive Manufacturing Letters* 13, no. November 2024 (2025): 100276, https://doi.org/10.1016/j.addlet.2025.100276.

44. K. K. Singh and R. Shrivastava, "Influence of Fiber Orientation on Thermo-Mechanical Response of Symmetric Glass/Epoxy Composite," *Journal of the Brazilian Society of Mechanical Sciences and Engineering* 45, no. 6 (2023): 288, https://doi.org/10.1007/s40430-023-04228-4.

45. Z. Wang, B. Zhang, J. Sun, and J. Wang, "Revealing the Process-Structure-Property Correlations in Fused Deposition Modeling of Short Fiber Filled Composites via Fiber Orientation Analysis," *Applied Composite Materials* 32, no. 2 (2025): 493–523, https://doi.org/10.1007/s10443-024-10279-0.

46. X. Wu, G. Ginoux, J. Paux, and S. Allaoui, "Influence of Temperature and Layer Height on the Structural and Mechanical Properties of Continuous Biocomposites by In–Nozzle Impregnation Additive Manufacturing," *Rapid Prototyping Journal* 31, no. 4 (2025): 893–907, https://doi.org/10.1108/RPJ-06-2024-0255.

47. J. Zhang, W. Yang, and Y. Li, "Process-Dependent Multiscale Modeling for 3D Printing of Continuous Fiber-Reinforced Composites," *Additive Manufacturing* 73 (2023): 103680, https://doi.org/10.1016/j.addma.2023.103680.

48. G. Ginoux, X. Wu, C. Laqraa, et al., "Continuous Additive Manufacturing of Hemp Yarn-Reinforced Biocomposites With Improved

Impregnation Method," *Composites Science and Technology* 251 (2024): 110561, https://doi.org/10.1016/j.compscitech.2024.110561.

49. K. Chen, L. Yu, Y. Cui, M. Jia, and K. Pan, "Optimization of Printing Parameters of 3D-Printed Continuous Glass Fiber Reinforced Polylactic Acid Composites," *Thin-Walled Structures* 164 (2021): 107717, https://doi.org/10.1016/j.tws.2021.107717.

50. M. Mohammadizadeh and I. Fidan, "Tensile Performance of 3D-Printed Continuous Fiber-Reinforced Nylon Composites," *Journal of Manufacturing and Materials Processing* 5, no. 3 (2021): 68, https://doi.org/10.3390/jmmp5030068.

51. E. H. Saidane, G. Arnold, P. Louis, and M. J. Pac, "3D Printed Continuous Glass Fibre-Reinforced Polyamide Composites: Fabrication and Mechanical Characterisation," *Journal of Reinforced Plastics and Composites* 41, no. 7–8 (2022): 284–295, https://doi.org/10.1177/07316844211051746.

52. H. Gharehbaghi, A. Shojaei, M. Sadeghzadeh, and A. Farrokhabadi, "Residual Stiffness and Strength Analysis of Fatigue Behavior in a 3D-Printed Honeycomb Structure of Continuous Glass Fiber-Reinforced Polylactic Acid (PLA) Composite," *Composites Part C: Open Access* 16 (2025): 100552, https://doi.org/10.1016/j.jcomc.2024.100552.